

Phase transitions and self-organized criticality in networks of stochastic spiking neurons

Ludmila Brochini¹, Ariadne de Andrade Costa², Miguel Abadi¹, Antônio C. Roque³, Jorge Stolfi², and Osame Kinouchi^{3,*}

¹Universidade de São Paulo, Departamento de Estatística-IME, São Paulo-SP, 05508-090, Brazil

²Universidade de Campinas, Instituto de Computação, Campinas-SP, 13083-852, Brazil

³Universidade de São Paulo, Departamento de Física-FFCLRP, Ribeirão Preto-SP, 14040-901, Brazil

*okinouchi@gmail.com

ABSTRACT

Phase transitions and critical behavior are crucial issues both in theoretical and experimental neuroscience. We report analytic and computational results about phase transitions and self-organized criticality (SOC) in networks with general stochastic neurons. The stochastic neuron has a firing probability given by a smooth monotonic function $\Phi(V)$ of the membrane potential V , rather than a sharp firing threshold. We find that such networks can operate in several dynamic regimes (phases) depending on the average synaptic weight and the shape of the firing function Φ . In particular, we encounter both continuous and discontinuous phase transitions to absorbing states. At the continuous transition critical boundary, neuronal avalanches occur whose distributions of size and duration are given by power laws, as observed in biological neural networks. We also propose and test a new mechanism to produce self-organized criticality (SOC): the use of dynamic neuronal gains – a form of short-term plasticity probably in the axon initial segment (AIS) – instead of depressing synapses at the dendrites (as previously studied in the literature). The new self-organization mechanism produces a slightly supercritical state, that we called SOSOC, in accord to some intuitions of Alan Turing.

Another simile would be an atomic pile of less than critical size: an injected idea is to correspond to a neutron entering the pile from without. Each such neutron will cause a certain disturbance which eventually dies away. If, however, the size of the pile is sufficiently increased, the disturbance caused by such an incoming neutron will very likely go on and on increasing until the whole pile is destroyed. Is there a corresponding phenomenon for minds, and is there one for machines? There does seem to be one for the human mind. The majority of them seems to be subcritical, i.e., to correspond in this analogy to piles of subcritical size. An idea presented to such a mind will on average give rise to less than one idea in reply. A smallish proportion are supercritical. An idea presented to such a mind may give rise to a whole "theory" consisting of secondary, tertiary and more remote ideas. (...) Adhering to this analogy we ask, "Can a machine be made to be supercritical?" Alan Turing (1950)¹.

Introduction

The Critical Brain Hypothesis^{2,3} states that (some) biological neuronal networks work near phase transitions because criticality enhances information processing capabilities⁴⁻⁶ and health⁷. The first discussion about criticality in the brain, in the sense that subcritical, critical and slightly supercritical branching process of thoughts could describe human and animal minds, has been made in the beautiful speculative 1950 Imitation Game paper by Turing¹. In 1995, Herz & Hopfield⁸ noticed that self-organized criticality (SOC) models for earthquakes were mathematically equivalent to networks of integrate-and-fire neurons, and speculated that perhaps SOC would occur in the brain. In 2003, in a landmark paper, these theoretical conjectures found experimental support by Beggs and Plenz⁹ and, by now, more than half a thousand papers can be found about the subject, see some reviews^{2,3}. Although not consensual, the Critical Brain Hypothesis can be considered at least a very fertile idea.

The open question about neuronal criticality is what are the mechanisms responsible for tuning the network towards the critical state. Up to now, the main mechanism studied is some dynamics in the links which, in the biological context, occur at the synaptic level¹⁰⁻¹³. Here we propose a whole new mechanism: dynamic neuronal gains, related to the diminution (and recovery) of the firing probability, an intrinsic neuronal property. The neuronal gain is experimentally related to the well known phenomenon of firing rate adaptation¹⁴⁻¹⁶. This new mechanism is sufficient to drive neuronal networks of stochastic neurons towards a critical boundary found,

by the first time, for these models. The neuron model we use was proposed by Galves and Locherbach¹⁷ as a stochastic model of spiking neurons inspired by the traditional integrate-and-fire (IF) model.

Introduced in the early 20th century¹⁸, IF elements have been extensively used in simulations of spiking neurons^{16,19–24}. Despite their simplicity, IF models have successfully emulated certain phenomena observed in biological neural networks, such as firing avalanches^{10,11,25} and multiple dynamical regimes^{26,27}. In these models, the membrane potential $V(t)$ integrates synaptic and external currents up to a *firing threshold* V_T ²⁸. Then, a spike is generated and $V(t)$ drops to a *reset potential* V_R . The *leaky integrate-and-fire* (LIF) model extends the IF neuron with a leakage current, which causes the potential $V(t)$ to decay exponentially towards a *baseline potential* V_B in the absence of input signals^{20,22}.

LIF models are deterministic but it has been claimed that stochastic models may be more adequate for simulation purposes²⁹. Some authors proposed to introduce stochasticity by adding noise terms to the potential^{20,21,26,27,29–33}, yielding the *leaky stochastic integrate-and-fire* (LSIF) models.

Alternatively, the Galves-Löcherbach (GL) model^{17,34–37} and also the model used by Larremore *et al.*³⁸ introduce stochasticity in their firing neuron models in a different way. Instead of noise inputs, they assume that the firing of the neuron is a random event, whose probability of occurrence in any time step is a *firing function* $\Phi(V)$ of membrane potential V . By subsuming all sources of randomness into a single function, the Galves-Löcherbach (GL) neuron model simplifies the analysis and simulation of noisy spiking neural networks.

Brain networks are also known to exhibit *plasticity*: changes in neural parameters over time scales longer than the firing time scale^{23,39}. For example, short-term synaptic plasticity⁴⁰ has been incorporated in models by assuming that the strength of each synapse is lowered after each firing, and then gradually recovers towards a reference value^{10,11}. This kind of dynamics drives the synaptic weights of the network towards critical values, a phenomenon called *self-organized criticality* (SOC), which is believed to optimize the network information processing^{3,4,7,9,41}.

In this work, first we study the dynamics of networks of GL neurons by a very simple and transparent mean-field calculation. We find both continuous and discontinuous phase transitions depending on the average synaptic strength and parameters of the firing function $\Phi(V)$. To the best of our knowledge, these phase transitions have never been observed in standard integrate-and-fire neurons. We also find that, at the second order phase transition the stimulated excitation of a single neuron causes avalanches of firing events (neuronal avalanches) that are similar to those observed in biological networks^{3,9}.

Second, we present a new mechanism for SOC based on a dynamics on the *neuronal gains* (a parameter of the neuron probably related to the axon initial segment – AIS^{28,42}), instead of depression of coupling strengths (related to neurotransmitter vesicle depletion at synaptic contacts between neurons) proposed in the literature^{10–13}. This new activity dependent gain model is sufficient to achieve self-organized criticality, both by simulation evidence and by mean-field calculations. The great advantage of this new SOC mechanism is that it is much more efficient—since we have only one adaptive parameter per neuron, instead of one per synapse.

The Model

We assume a network of N GL neurons that change states in parallel at certain *sampling times* with a uniform spacing Δ . Thus, the membrane potential of neuron i is modeled by a real variable $V_i[t]$ indexed by *discrete time* t , an integer that represents the sampling time $t\Delta$.

Each synapse transmits signals from some *presynaptic* neuron j to some *postsynaptic* neuron i , and has a *synaptic strength* w_{ij} . If neuron j fires between discrete times t and $t + 1$, its potential drops to $V_R = 0$. This event increments by w_{ij} the potential of every postsynaptic neuron i that does not fire in that interval. The potential of a non-firing neuron may also integrate an *external stimulus* $I_i[t]$, which can model signals received from sources outside the network. Apart from these increments, the potential of a non-firing neuron decays at each time step towards the baseline voltage V_B by a factor $\mu \in [0, 1]$, which models the effect of a leakage current. Since the zero of potential is arbitrary, we assume $V_B = 0$.

We introduce the Boolean variable $X_i[t] \in \{0, 1\}$ which denotes whether neuron i fired between t and $t + 1$. The potentials evolve as:

$$V_i[t + 1] = \begin{cases} V_R & \text{if } X_i[t] = 1, \\ \mu V_i[t] + I_i[t] + \sum_{j=1}^N w_{ij} X_j[t] & \text{if } X_i[t] = 0. \end{cases} \quad (1)$$

This corresponds to a GL neuron with a geometric leakage function $g[t - t_s] = \mu^{[t - t_s]}$, where t_s is the time of the last spike of neuron i , see¹⁷. We have $X_i[t + 1] = 1$ with probability $\Phi(V_i[t])$, which is called the *firing function*^{17,34–38}. We also have $X_i[t + 1] = 0$ if $X_i[t] = 1$ (refractory period). The function Φ is sigmoidal, that is, monotonically increasing, with limiting values $\Phi(-\infty) = 0$ and $\Phi(+\infty) = 1$, with only one derivative maximum. We also assume that $\Phi(V)$ is zero up to some *threshold potential* V_T . If Φ is the shifted Heaviside step function Θ , $\Phi(V) = \Theta(V - V_T)$, we have a deterministic discrete-time LIF neuron. Any other choice for $\Phi(V)$ gives a stochastic neuron.

The network activity is measured by the fraction (or density) $\rho[t]$ of firing neurons:

$$\rho[t] = \frac{1}{N} \sum_{j=1}^N X_j[t]. \quad (2)$$

The density $\rho[t]$ can be computed from the probability density $p[t](V)$ of potentials at time t :

$$\rho[t] = \int_{V_T}^{\infty} \Phi(V) p[t](V) dV, \quad (3)$$

where $p[t](V) dV$ is the fraction of neurons with potential in the range $[V, V + dV]$ at time t .

Neurons that fire between t and $t + 1$ have their potential reset to zero. They contribute to $p[t + 1](V)$ a Dirac impulse at potential V_R , with amplitude (integral) $\rho[t]$ given by equation (3). In subsequent time steps, the potentials of all neurons will evolve according to equation (1). This process modifies $p[t](V)$ also for $V \neq V_R$.

Results

In this paper we study only fully connected networks, that is, all neurons have $N - 1$ neighbors. In this case, to obtain sensible results, we must scale the synapses as $w_{ij} = W_{ij}/N$, where the random variables W_{ij} have finite mean W and finite variance. We also study only the case with $V_R = 0$ and $I_i[t] = I$ (constant uniform input). So, for these networks, equation (1) reads:

$$V_i[t + 1] = \begin{cases} 0 & \text{if } X_i[t] = 1, \\ \mu V_i[t] + I + \frac{1}{N} \sum_{j=1}^N W_{ij} X_j[t] & \text{if } X_i[t] = 0. \end{cases} \quad (4)$$

Mean-field calculation

In the mean-field analysis, we assume that the synaptic weights W_{ij} follow a distribution with average W and finite variance. The mean-field approximation disregards correlations, so the final term of equation (1) becomes:

$$\frac{1}{N} \sum_{j=1}^N W_{ij} X_j[t] = W \rho[t]. \quad (5)$$

Notice that the variance of the weights W_{ij} becomes immaterial when N tends to infinity.

By now, we assume that the external input I is zero for all neurons and all times. Therefore, every neuron i that does not fire between t and $t + 1$ (that is, with $X_i[t] = 0$) has its potential changed in the same way:

$$V_i[t + 1] = \mu V_i[t] + W \rho[t], \quad (6)$$

Recall that the probability density $p[t](V)$ has a Dirac impulse at potential $U_0 = 0$, representing all neurons that fired in the previous interval. This Dirac impulse is modified in later steps by equation (6). It follows that, once all neurons have fired at least once, the density $p[t](V)$ will be a combination of discrete impulses with amplitudes $\eta_0[t], \eta_1[t], \eta_2[t], \dots$, at potentials $U_0[t], U_1[t], U_2[t], \dots$, such that $\sum_{k=0}^{\infty} \eta_k = 1$.

The amplitude $\eta_k[t]$ is the fraction of neurons with *firing age* k at discrete time t , that is, neurons that fired between times $t - k - 1$ and $t - k$, and did not fire between $t - k$ and t . The common potential of those neurons, at time t ,

is $U_k[t]$. In particular, $\eta_0[t]$ is the fraction $\rho[t-1]$ of neurons that fired in the previous time step. For this type of distribution, the integral of equation (3) becomes a discrete sum:

$$\rho[t] = \sum_{k=0}^{\infty} \Phi(U_k[t]) \eta_k[t]. \quad (7)$$

According to equation (6), the values $\eta_k[t]$ and $U_k[t]$ evolve by the equations

$$\eta_k[t+1] = (1 - \Phi(U_{k-1}[t])) \eta_{k-1}[t], \quad (8)$$

$$U_k[t+1] = \mu U_{k-1}[t] + W\rho[t], \quad (9)$$

for all $k \geq 1$, with $\eta_0[t+1] = \rho[t]$ and $U_0[t+1] = 0$.

Stationary states for general Φ and μ

A *stationary state* is a density $p[t](V) = p(V)$ of membrane potentials that does not change with time. In such a regime, quantities U_k and η_k do not depend anymore on t . Therefore, the equations (8–9) become the recurrence equations $\eta_0 = \rho = \sum_{k=0}^{\infty} \Phi(U_k)\eta_k$, $U_0 = 0$, and :

$$\eta_k = (1 - \Phi(U_{k-1})) \eta_{k-1}, \quad (10)$$

$$U_k = \mu U_{k-1} + W\rho, \quad (11)$$

for all $k \geq 1$.

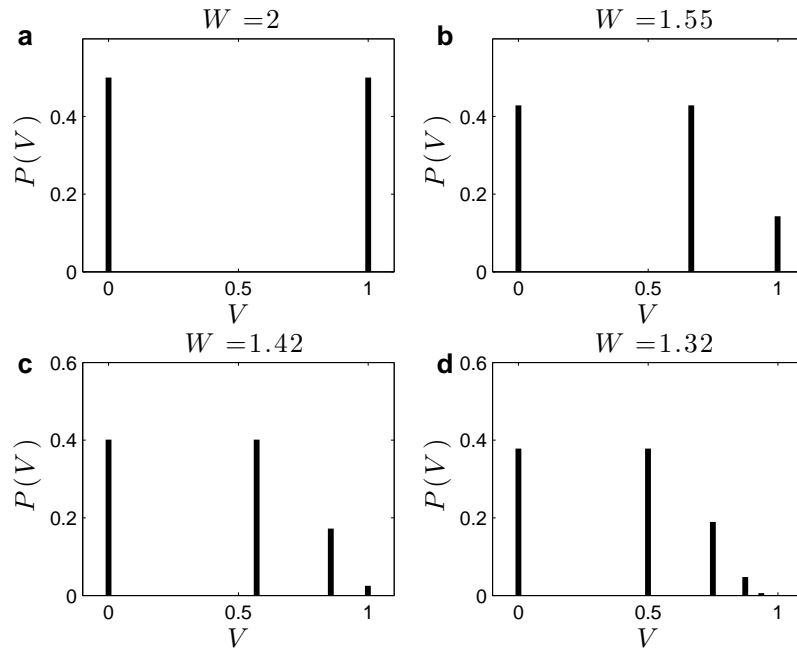


Figure 1. Examples of stationary potential distributions $P(V)$: monomial Φ function with $r = 1, \gamma = 1, \mu = 1/2$ case with different values of W . a) $W_2 = W_B = 2$, two peaks; b) $W_3 = 14/9$, three peaks; c) $W_4 = 488/343$, four peaks, d) $W_\infty \approx 1.32$, infinite number of peaks with $U_\infty = 1$. Notice that for $W < W_\infty$ all the peaks in the distribution $p(V)$ lie at potentials $U_k < 1$. For $W_B = 2$ we have $\eta_0 = \eta_1 = 1/2$, producing a bifurcation to a 2-cycle. The values of $W_m = W_2, W_3, W_4$ and W_∞ can be obtained analytically by imposing the condition $U_m = 1$ in equations (10–11).

Since equations (10) are homogeneous on the η_k , the normalization condition $\sum_{k=0}^{\infty} \eta_k = 1$ must be included explicitly. So, integrating over the density $p(V)$ leads to a discrete distribution $P(V)$ (see Fig. 1 for a specific Φ).

Equations (10–11) can be solved numerically, e. g. by simulating the evolution of the potential probability density $p[t](V)$ according to equation (8–9), starting from an arbitrary initial distribution, until reaching a stable distribution (the probabilities η_k should be renormalized for unit sum after each time step, to compensate for rounding errors).

The monomial saturating Φ with $\mu > 0$

Now we consider a specific class of firing functions, the *saturating monomials*. This class is parametrized by a positive *degree* r and a *neuronal gain* $\gamma > 0$. In all functions of this class, $\Phi(V)$ is 0 when $V \leq V_T$, and 1 when $V \geq V_S$, where the saturation potential is $V_S = V_T + 1/\gamma$. In the interval $V_T < V < V_S$ we have the monomial:

$$\Phi(V) = (\gamma(V - V_T))^r. \quad (12)$$

Note that these functions can be seen as limiting cases of sigmoidal functions, and that we recover the deterministic LIF model $\Phi(V) = \Theta(V - V_T)$ when $\gamma \rightarrow \infty$. Notice that for such saturating monomials, there is a value $W_B = V_T + 2/\gamma$ above which the dynamics is deterministic, leading to the *2-cycles*, see Appendix. The case of isolated neurons with the monomial saturating Φ is also studied in the Appendix.

In the analyses that follows, the control parameters are W and γ , and $\rho(W, \gamma)$ is the order parameter. We obtain numerically $\rho(W, \gamma)$ and the phase diagram (W, γ) for several values of $\mu > 0$, for the linear ($r = 1$) saturating Φ with $V_T = 0$ (Fig. 2). Only the first 100 peaks (U_k, η_k) were considered, since, for the given μ and Φ , there was no significant probability density beyond that point. The same numerical method can be used for $r \neq 1, V_T \neq 0$.

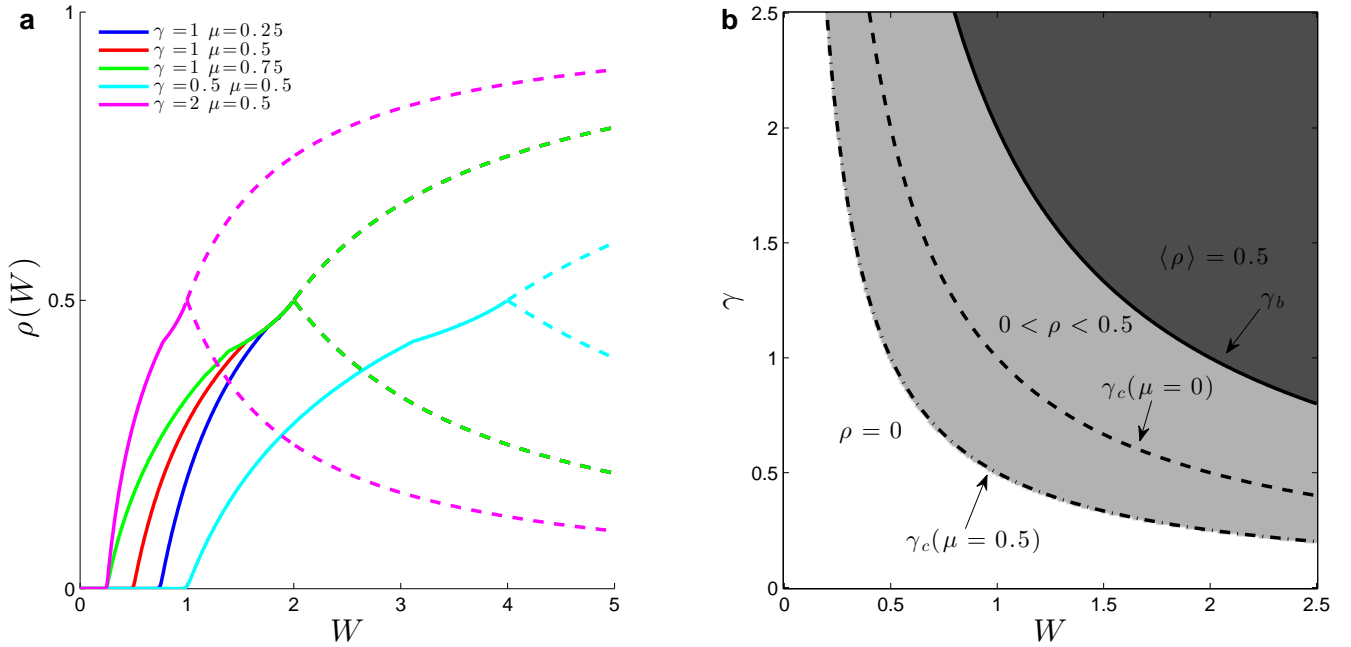


Figure 2. Results for $\mu > 0$: a) Numerically computed $\rho(W)$ curves with $r = 1$ and $(\gamma, \mu) = (1, 1/4), (1, 1/2), (1, 3/4), (1/2, 1/2), (2, 1/2)$. The absorbing state ρ_0 loses stability at W_C and the non trivial fixed point $\rho > 0$ appears. At $W_B = 2/\gamma$, we have $\rho = 1/2$ and from there *2-cycles* appear in the form $\rho[t + 1] = 1 - \rho[t]$, where $\rho[t]$ can have any value in the region bounded between the trace $\rho_1/(\gamma W)$ lines $\rho_2 = (W - 1/\gamma)/W$, see Eq. 31 of the Appendix. b) Numerically computed (γ, W) diagram showing the critical boundaries $\gamma_c(W) = (1 - \mu)/W$ and the bifurcation line $\gamma_B(W) = 2/W$ to *2-cycles*.

Near the critical point, we obtain numerically $\rho(W, \mu) \approx C(W - W_C)/W$, where $W_C(\gamma) = (1 - \mu)/\gamma$ and $C(\mu)$ is a constant. So, the critical exponent is $\alpha = 1$, characteristic of the mean-field directed percolation (DP) universality class^{3,4}. The critical boundary in the (W, γ) plane, numerically obtained, seems to be $\gamma_c(W) = (1 - \mu)/W$ (Fig. 2b).

Analytic results for $\mu = 0$

Below we give results of a simple mean-field analysis in the limits $N \rightarrow \infty$ and $\mu \rightarrow 0$. The latter implies that, at time $t + 1$, the neuron “forgets” its previous potential $V_i[t]$ and integrates only the inputs $I[t] + W_{ij}X_j[t]$. This scenario is interesting because it enables analytic solutions, yet exhibits all kinds of behaviors and phase transitions that occur with $\mu > 0$.

When $\mu = 0$ and $I_i[t] = I$ (uniform constant input), the density $p[t](V)$ consists of only two Dirac peaks at potentials $U_0[t] = V_R = 0$ and $U_1[t] = I + W\rho[t - 1]$, with fractions $\eta_0[t]$ and $\eta_1[t]$ that evolve as:

$$\eta_0[t + 1] = \rho[t] = \Phi(0)\eta_0[t] + \Phi(I + W\eta_0[t])(1 - \eta_0[t]), \quad (13)$$

$$\eta_1[t + 1] = 1 - \eta_0[t + 1]. \quad (14)$$

Furthermore, if neurons have not spontaneous firing, that is, $\Phi(0) = 0$, then equation (13) reduces to:

$$\eta_0[t + 1] = \rho[t] = \Phi(I + W\eta_0[t])(1 - \eta_0[t]). \quad (15)$$

In a stationary regime, equation (15) simplifies to:

$$\rho = (1 - \rho)\Phi(I + W\rho), \quad (16)$$

since $\eta_0 = \rho$, $\eta_1 = 1 - \rho$, $U_0 = 0$, and $U_1 = I + W\rho$. Below, all the results refer to the monomial saturating Φ s (Fig. 3a).

Continuous phase transitions in networks: the case with $r = 1$.

When $r = 1$, we have the linear function $\Phi(V) = \gamma V$ for $0 < V < V_S = 1/\gamma$. The stationary state condition equation (16) then becomes:

$$\gamma W\rho^2 + (1 - \gamma W)\rho = 0. \quad (17)$$

The two solutions are the absorbing state $\rho = 0$ and the non-trivial state:

$$\rho = \frac{W - W_C}{W}, \quad (18)$$

with $W_C = 1/\gamma$. Since we must have $0 < \rho \leq 1/2$, this solution is valid only for $W_C < W \leq W_B = 2/\gamma$ (Fig 3b).

This solution describes an stationary state where $1 - \rho$ of the neurons are at potential $U_1 = W - W_C$. The neurons that will fire in the next step are a fraction $\Phi(U_1)$ of those, which are again a fraction ρ of the total. For any $W > W_C$, the state $\rho = 0$ is unstable: any small perturbation of the potentials cause the network to converge to the active stationary state above. For $W < W_C$, the solution $\rho = 0$ is stable and absorbing. In the $\rho(W)$ plot, the locus of stationary regimes defined by equation (18) bifurcates at $W = W_B$ into the two bounds of equation (31) that delimit the *2-cycles* (Fig. 3b).

So, at the critical boundary $W = 1/\gamma$, we have a standard continuous absorbing state transition $\rho(W) \propto (W - W_C)^\alpha$ with a critical exponent $\alpha = 1$, which also can be written as $\rho(\gamma) \propto (\gamma - \gamma_C)^\alpha$. In the (γ, W) plane, the phase transition corresponds to a critical boundary $\gamma_C(W) = 1/W$, below the *2-cycle* phase transition $\gamma_B(W) = 2/W$ (Fig. 3c).

Discontinuous phase transitions in networks: the case with $r > 1$.

When $r > 1$ and $W \leq W_B = 2/\gamma$, the stationary state condition is:

$$(\gamma W)^r \rho^r - (\gamma W)^r \rho^{r-1} + 1 = 0. \quad (19)$$

This equation has a non trivial solution ρ^+ only when $1 \leq r \leq 2$ and $W_C(r) \leq W \leq W_B$, for a certain $W_C(r) > 1/\gamma$. In this case, at $W = W_C(r)$, there is a discontinuous (first-order) phase transition to a regime with activity $\rho = \rho_C(r) \leq 1/2$ (Fig. 3d). It turns out that $\rho_C(r) \rightarrow 0$ as $r \rightarrow 1$, recovering the continuous phase transition in that limit. For $r = 2$, the solution to equation (19) is a single point $\rho(W_C) = \rho_C = 1/2$ at $W_C = 2/\gamma = W_B$ (Fig. 3f).

Notice that, in the linear case, the fixed point $\rho_0 = \rho = 0$ is unstable for $W > 1$ (Fig. 3b). This occurs because the *separatrix* ρ_- (trace lines, Fig. 3d), for $r \rightarrow 1$, collapses with the ρ_0 point, so that it loses its stability.

It also occurs discontinuous transitions if we have a non zero firing threshold V_T . Analytic results for $\mu = 0, V_T > 0, I > 0$ are given in the Appendix.

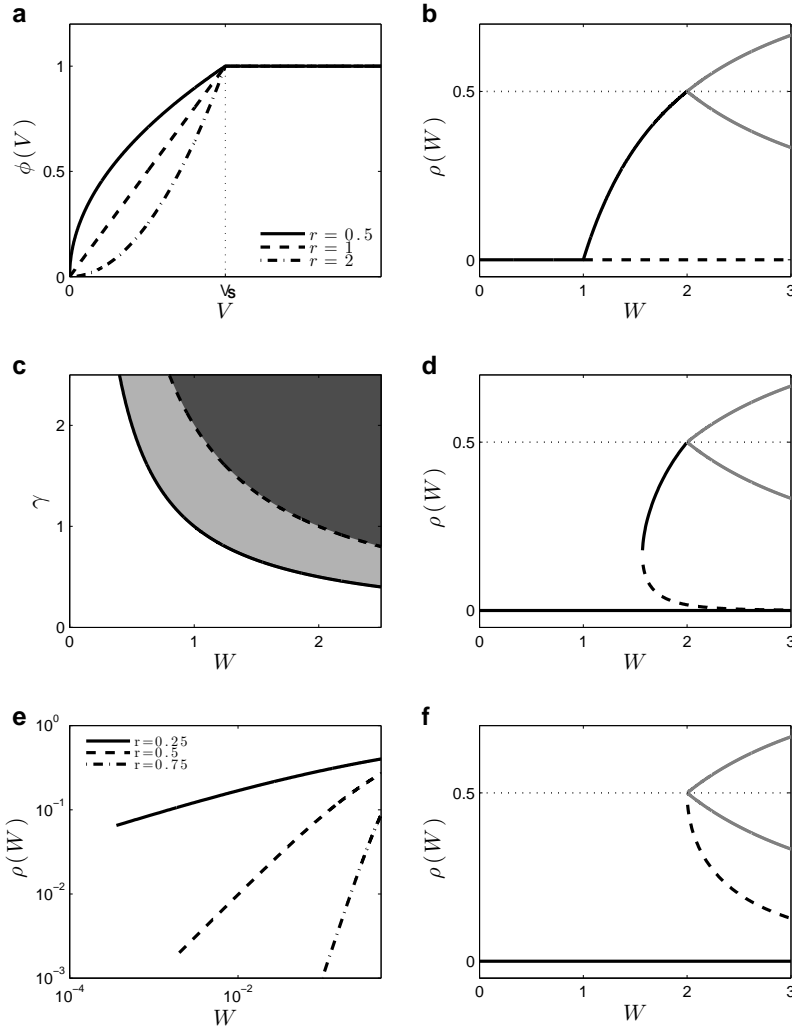


Figure 3. Firing densities (with $\gamma = 1$) and phase diagram with $\mu = 0$ and $V_T = 0$. a) Examples of monomial firing functions $\Phi(V)$ with $\gamma = 1$ $r = 0.5, 1$ and 2 . b) The $\rho(W)$ bifurcation plot for $r = 1$. The absorbing state ρ_0 loses stability after $W > W_C = 1$ (dashed line). The non trivial fixed point ρ^+ bifurcates at $W_B = 2/\gamma = 2$ into two branches (gray lines) that bound the marginally stable 2-cycles. c) The (γ, W) phase diagram for $r = 1$. Below the critical boundary $\gamma = \gamma_C(W) = 1/W$ the inactive state $\rho = 0$ is absorbing and stable; above that line it is also absorbing but unstable. Above the line $\gamma = \gamma_B(W) = 2/W$ there are only the marginally stable 2-cycles. For $\gamma_C(W) < \gamma \leq \gamma_B(W)$ there is a single stationary regime $\rho(W) = (W - W_C)/W < 1/2$, with $W_C = 1/\gamma$. d) Discontinuous phase transitions for $\gamma = 1$ with exponents $r = 1.2$. The absorbing state ρ_0 now is stable (solid line at zero). The non trivial fixed point ρ^+ starts with the value ρ_C at W_C and bifurcates at W_B , creating the boundary curves (gray) that delimit possible 2-cycles. At W_C also appears the unstable separatrix ρ_- (dashed line). e) Ceaseless activity (no phase transitions) for $r = 0.25, 0.5$ and $r = 0.75$. The activity approach zero (for $W = 0$ as power laws. f) In the limiting case $r = 2$ we do not have a $\rho > 0$ fixed point, but only the stable $\rho = 0$ (black), the 2-cycles region (gray) and the unstable separatrix (traces).

Ceaseless activity: the case with $r < 1$.

When $r < 1$, there is no absorbing solution $\rho = 0$ to equation (19). In the $W \rightarrow 0$ limit we get $\rho(W) = (\gamma W)^{r/(1-r)}$. These power laws means that $\rho > 0$ for any $W > W_C(r) = 0$ (Fig. 3e). We recover the second order transition $W_C(r = 1) = 1/\gamma$ when $r \rightarrow 1$ in equation (19). Interestingly, this ceaseless activity $\rho > 0$ for any $W > 0$ seems to

be similar to that found by Larremore *et al.*³⁸ with a $\mu = 0$ linear saturating model. This ceaseless activity, even with $r = 1$, perhaps is due to the presence of inhibitory neurons in Larremore *et al.* model.

Neuronal avalanches

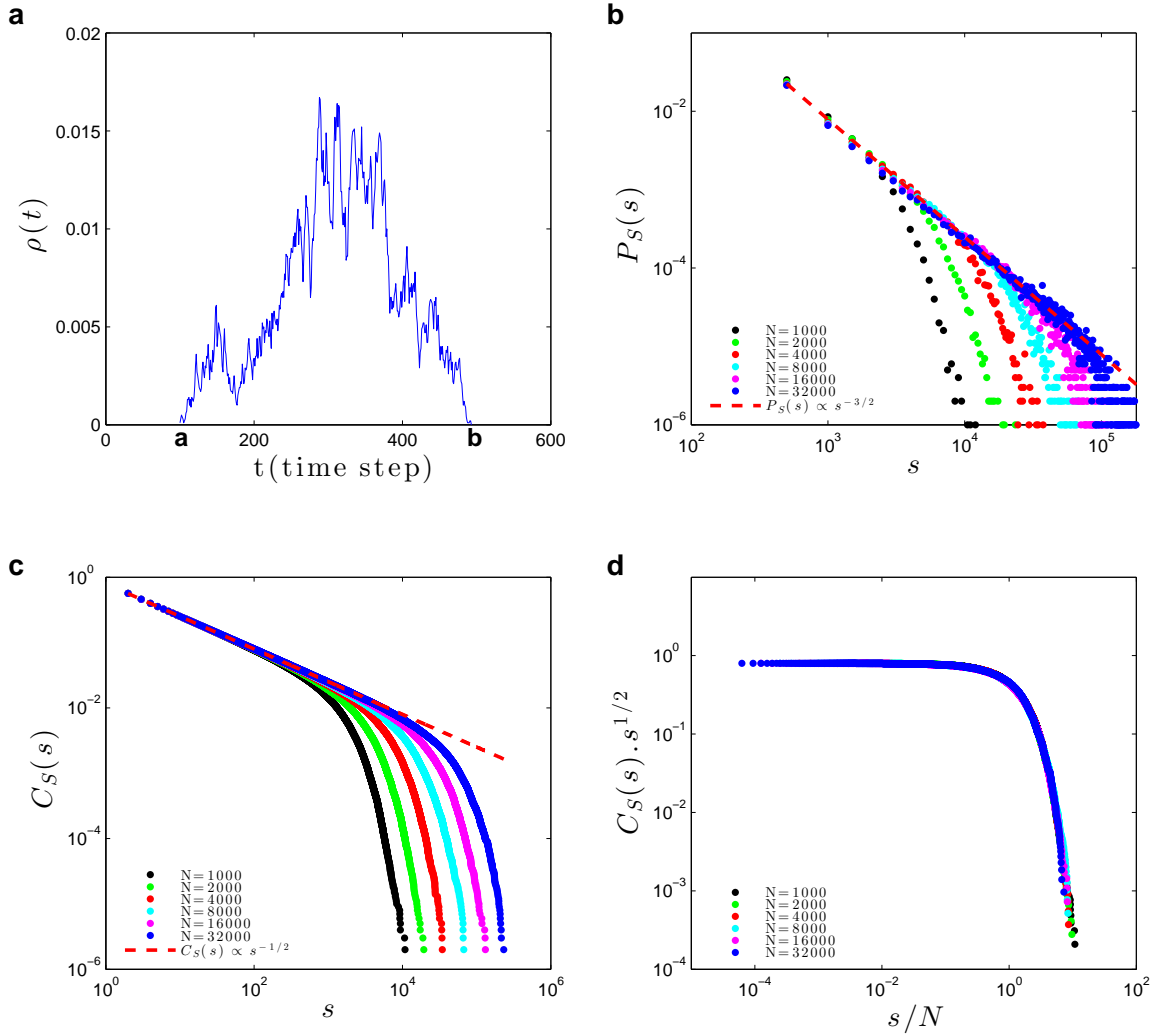


Figure 4. Avalanche size statistics in the static model: Simulations at the critical point $W_C = 1, \gamma_C = 1$ (with $\mu = 0$). a) Example of avalanche profile $\rho[t]$ at the critical point. b) Avalanche size distribution $P_S(s) \equiv P(S = s)$, for network sizes $N = 1000, 2000, 4000, 8000, 16000$ and 32000 . The dashed reference line is proportional to $s^{-\beta}$, with $\beta = 3/2$. c) Complementary cumulative distribution $C_S(s) = \sum_k^\infty P_S(k)$. Being an integral of $P_S(s)$, its power law exponent is $-\beta + 1 = -1/2$ (dashed line). d) Data collapse (finite-size scaling) for $C_S(s)s^{1/2}$ versus function of s/N^{c_S} , with the cutoff exponent $c_S = 1$.

Firing avalanches in neural networks have attracted significant interest because of their possible connection to efficient information processing^{3-5,7,9}. Through simulations, we studied the critical point $W_C = 1, \gamma_C = 1$ (with $\mu = 0$) in search for neuronal avalanches^{3,9} (Fig 4).

An avalanche that starts at discrete time $t = a$ and ends at $t = b$ has duration $d = b - a$ and size $s = N \sum_{t=a}^b \rho[t]$ (Fig. 4a). By using the notation S for a random variable and s for its numerical value, we observe a power law avalanche size distribution $P_S(s) \equiv P(S = s) \propto s^{-\beta}$, with the mean-field exponent $\beta = 3/2$ (Fig. 4b)^{3,9,11}. Since

the distribution $P_S(s)$ is noisy for large s , for further analysis we use the complementary cumulative function $C_S(s) \equiv P(S \geq s) = \sum_{k=s}^{\infty} P_S(k)$ (which gives the probability of having an avalanche with size equal or greater than s) because it is very smooth and monotonic (Fig. 4c). Data collapse gives a finite-size scaling exponent $c_S = 1$ (Fig. 4d)^{12,13}.

We also observed a power law distribution for avalanche duration, $P_D(d) \equiv P(D = d) \propto d^{-\delta}$ with $\delta = 2$ (Figure 5a). The complementary cumulative distribution is $C_D(d) \equiv P(D \geq d) = \sum_{k=d}^{\infty} P_D(k)$. From data collapse, we find a finite-size scaling exponent $c_D = 1/2$ (Fig. 5b), in accord with the literature¹¹.

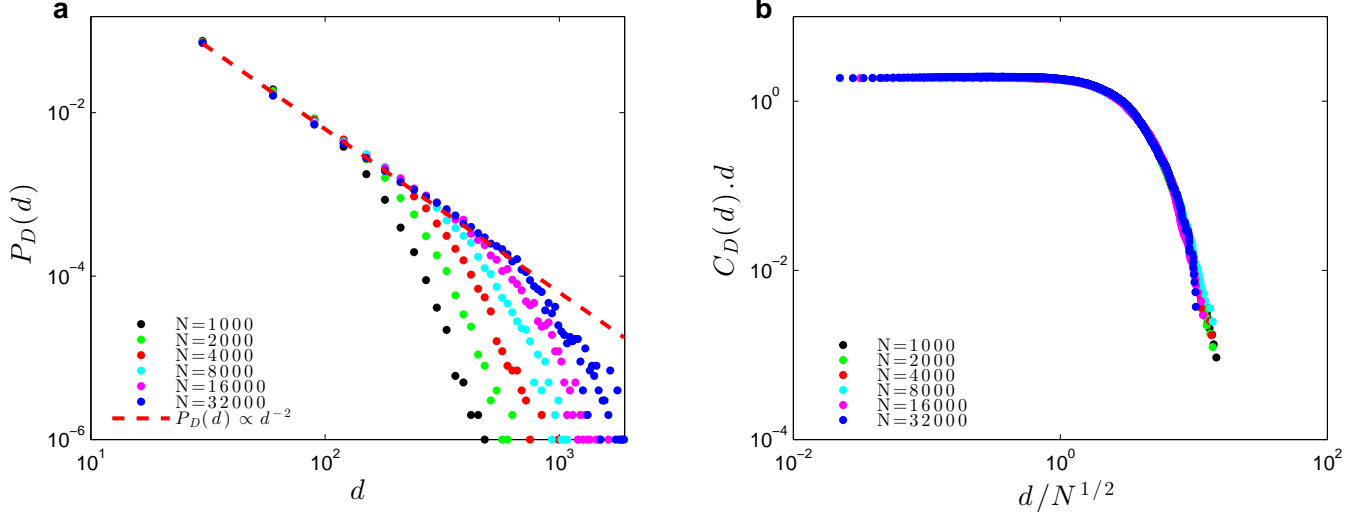


Figure 5. Avalanche duration statistics in the static model: Simulations at the critical point $W_C = 1, \gamma = 0$ ($\mu = 0$) for network sizes $N = 1000, 2000, 4000, 8000, 16000$ and 32000 : a) Probability distribution $P_D(d) \equiv P(D = d)$ for avalanche duration d . The dashed reference line is proportional to $d^{-\delta}$, with $\delta = 2$. b) Data collapse $C_D(d)d$ versus d/N^{c_D} , with the cutoff exponent $c_D = 1/2$. The complementary cumulative function $C_D(d) \equiv \sum_k^{\infty} P_D(k)$, being an integral of $P_D(d)$, has power law exponent $-\delta + 1 = -1$.

The model with dynamic parameters

The results of the previous section were obtained by fine-tuning the network at the critical point $\gamma_C = W_C = 1$. Given the conjecture that the critical situation has functional advantages, a biological model should include some homeostatic mechanism capable of tuning the network towards criticality. Without such mechanism, we cannot truly say that the network self-organizes toward the critical regime.

However, observing that the relevant parameter for criticality in our model is the critical boundary $\gamma_C W_C = 1$, we propose to work with dynamic gains $\gamma_i[t]$ while keeping the synapses W_{ij} fixed. The idea is to reduce the gain $\gamma_i[t]$ when the neuron fires, and let the gain slowly recover towards a higher resting value after that:

$$\gamma_i[t+1] = \gamma_i[t] + \frac{1}{\tau} (A - \gamma_i[t]) - u \gamma_i[t] X_i[t]. \quad (20)$$

Now, the factor τ is related to the characteristic recovery time of the gain, A is the asymptotic resting gain, and $u \in [0, 1]$ is the fraction of gain lost due to the firing. This model is plausible biologically, and can be related to a decrease and recovery, due to the neuron activity, of the firing probability at the AIS⁴². Our dynamic $\gamma_i[t]$ mimic the well known phenomenon of *spike firing adaptation*^{14,15}.

This approach seems sufficient to achieve a state very similar to self-organized criticality. Fig. 6a shows a simulation with all-to-all coupled networks with N neurons and, for simplicity, $W_{ij} = W$. We observe that the average gain $\gamma[t] = \frac{1}{N} \sum_{i=1}^N \gamma_i[t]$ seems to converge toward the critical value $\gamma_C(W) = 1/W = 1$, starting from different $\gamma[0] \neq 1$. As the network converges to the critical state, we observe power-law avalanche size distributions with exponent $-3/2$ leading to a cumulative function $C_S(s) \propto s^{-1/2}$ (Fig. 6b). Curiously, the finite-size scaling exponent is $c_S = 2/3$, which is different from that observed in the static model with fixed gains ($c_S = 1$) (Fig. 4d).

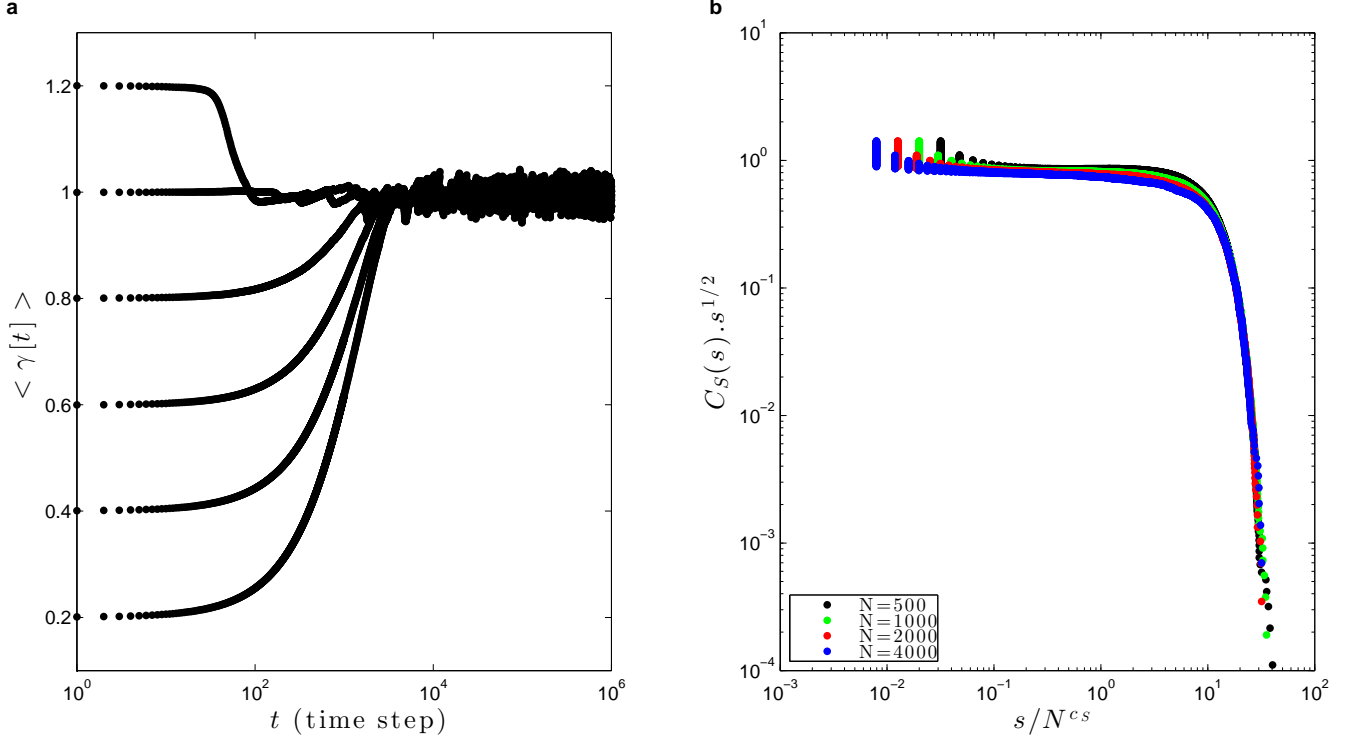


Figure 6. Self-organization with dynamic neuronal gains: Simulations of a network of GL neurons with fixed $W_{ij} = W = 1, \gamma = 1, u = 1, A = 1.1$ and $\tau = 1000$ ms. Dynamic gains $\gamma_i[t]$ starts with $\gamma_i[0]$ uniformly distributed in $[0, \gamma_{\max}]$. The average initial condition is $\gamma[t] \equiv \frac{1}{N} \sum_i^N \gamma_i[t] \approx \gamma_{\max}/2$, which produces the different initial conditions $\gamma[0]$. (a) Self-organization of the average gain $\gamma[t]$ over time. The horizontal dashed line marks the value $\gamma_c = 1$. (b) Data collapse for $C_S(s)s^{1/2}$ versus s/N^{c_S} for several N , with the cutoff exponent $c_S = 2/3$.

This empirical evidence is supported by a mean-field analysis of equation (20). Averaging over the sites, we have for the average gain:

$$\gamma[t+1] = \gamma[t] + \frac{1}{\tau} (A - \gamma[t]) - u\rho[t]\gamma[t]. \quad (21)$$

In the stationary state, we have $\gamma[t+1] = \gamma[t] = \gamma^*$, so:

$$\left(\frac{1}{\tau} + u\rho^* \right) \gamma^* = \frac{A}{\tau}. \quad (22)$$

But we have the relation

$$\rho^* = C(\gamma^* - \gamma_c)/\gamma^* \quad (23)$$

near the critical region, where C is a constant that depends on $\Phi(V)$ and μ , for example, with $\mu = 0$, $C = 1$ for Φ linear monomial model. So:

$$\left(\frac{\gamma^*}{\tau} + uC\gamma^* - uC\gamma_c \right) \gamma^* = \frac{A\gamma^*}{\tau}. \quad (24)$$

Eliminating the common factor γ^* , and dividing by uC , we have:

$$\left(1 + \frac{1}{uC\tau} \right) \gamma^* = \gamma_c + \frac{A}{uC\tau}. \quad (25)$$

Now, call $x = 1/(uC\tau)$. Then, we have:

$$\gamma^* = \frac{\gamma_C + Ax}{1+x}. \quad (26)$$

The fine tuning solution is to put by hand $A = \gamma_C$, which leads to $\gamma^* = \gamma_C$ independent of x . This fine tuning solution should not be allowed in a true SOC scenario. So, suppose that $A = B\gamma_C$. Then, we have:

$$\gamma^* = \gamma_C \frac{1+Bx}{1+x}. \quad (27)$$

Now we see that, to have a critical or supercritical state (where equation (23) holds), we must have $B > 1$, otherwise we fall in the subcritical state $\gamma^* < \gamma_C$ where $\rho^* = 0$ and this mean-field calculation is not valid. A first order approximation leads to:

$$\gamma^* = \gamma_C + (A - \gamma_C)x + O(x^2). \quad (28)$$

This mean-field calculation shows that, if $x \rightarrow 0$, we obtain a SOC state $\gamma^* \rightarrow \gamma_C$. However, the strict case $x \rightarrow 0$ would require a scaling $\tau = O(N^a)$ with an exponent $a > 0$, as done previously for dynamic synapses in¹⁰⁻¹³, This scaling is necessary because all-to-all networks are pathological: the same pathology imply the scaling $w_{ij} = W_{ij}/N$, which is also non-biological since depends on the non-local information given by N . This dependence on N is similar to the scaling J_{ij}/N for magnetic couplings in spin systems with all-to-all networks, which also is non-physical.

However, if we want to avoid the non-biological factor $\tau(N) = O(N^a)$, we can use reasonable parameters as $\tau \in [10, 100]$ ms, $u = [0.1, 1]$, $C = 1$ and $A \in [1.1, 2]\gamma_C$. In particular, if $\tau = 100, u = 1$ and $A = 1.1$, we have $x = 0.01$ and:

$$\gamma^* = 1.001\gamma_C + O(10^{-4}). \quad (29)$$

Even a more conservative value $\tau = 10$ ms gives $\gamma^* = 1.01\gamma_C$. Although not perfect SOC, this result is totally sufficient to explain power law neuronal avalanches. We call this phenomena self-organized supercriticality (SOSC), where the supercriticality can be very small.

We must yet to determine the volume of parameter space (τ, A, u) where the SOSC phenomenon holds. In the case of dynamic synapses $W_{ij}[t]$, this parametric volume is very large^{12,13} and we conjecture that the same occurs for the dynamic gains $\gamma[t]$. This shall be studied in detail in another paper.

Discussion

Stochastic model: The stochastic neuron introduced by Galves and Löcherbach^{17,37} are interesting elements for studies of networks of spiking neurons because they enable exact analytic results and simple numerical calculations. While the LSIF models of Soula *et al.*³⁰ and Cessac³¹⁻³³ introduce stochasticity in the neuron's behavior by adding noise terms to its potential, the GL model is agnostic about the origin of noise and randomness (which can be a good thing when several noise sources are present). All the random behavior is grouped at the single firing function $\Phi(V)$.

Phase transitions: Networks of GL neurons display a variety of dynamical states with interesting phase transitions. We looked for stationary regimes in such networks, for some specific firing functions $\Phi(V)$ with no spontaneous activity at the baseline potential (that is, with $\Phi(0) = 0$ and $I = 0$). We studied the changes in those regimes as a function of the mean synaptic weight W and mean neuronal gain γ . We found basically tree kinds of phase transition, depending of the behavior of $\Phi(V) \propto V^r$ for low V :²⁻⁴:

$r < 1$: A ceaseless dynamic regime with no phase transitions ($W_C = 0$) similar to that found by Larremore (2014);

$r = 1$: A continuous (second order) absorbing state phase transition in the Directed Percolation universality class usual in SOC models^{2,3,12,13};

$r > 1$: Discontinuous (first order) absorbing state transitions.

We also observed discontinuous phase transitions for any $r > 0$ when the neurons have a firing threshold $V_T > 0$, see Appendix.

The deterministic LIF neuron models, which do not have noise, do not seem to allow these kinds of transitions^{23,26,27}. The model studied by Larremore *et al.*³⁸ is equivalent to the GL model with monomial saturating firing function with $r = 1, V_T = 0$ and $\gamma = 1$. They did not report any phase transition (perhaps because of the effect of inhibitory neurons in their network), but found a ceaseless activity very similar to what we observed with $r < 1$.

Avalanches: In the case of second-order phase transitions ($\Phi(0) = 0, r = 1, V_T = 0$), we detected firing avalanches at the critical boundary $\gamma_C = 1/W$, whose size and duration power law distributions present the standard mean-field exponents $\beta = 3/2$ and $\delta = 2$. We observed a very good finite-scaling and data collapse behavior, with finite-size exponents $c_S = 1$ and $c_D = 1/2$.

Self-organized criticality:

One way to achieve this goal is to use dynamical synapses $W_{ij}[t]$, in a way that mimics the loss of strength after a synaptic discharge (presumably due to neurotransmitter vesicles depletion), and the subsequent slow recovery¹⁰⁻¹³:

$$W_{ij}[t+1] = W_{ij}[t] + \frac{1}{\tau N K_j} (A - W_{ij}[t]) - u W_{ij}[t] X_j[t]. \quad (30)$$

where K_j is the number of neighbors of the presynaptic neuron j . Parameters are related to the synaptic recovery time τ , the asymptotic value A and u the fraction of synaptic lost after firing. This has been examined in¹⁰⁻¹³. For our all-to-all coupled network, we have $K = N - 1$ and $N(N - 1)$ dynamic equations for the W_{ij} s. This is a huge number, for example $O(10^8)$ equations, even for a moderate network of $N = 10^4$ neurons^{12,13}. The possibility of well behaved SOC in bulk dissipative systems with loading is discussed in^{11,43}. Further considerations for systems with conservation in average at the stationary state, as occurs in our model, are made in^{12,13}.

Inspired by the presence of the critical boundary, we proposed a new mechanism for short-scale neural network plasticity, based on dynamic neuron gains $\gamma_i[t]$ instead of the above dynamic synaptic weights. This new mechanism is biologically plausible, probably related an activity-dependent firing probability at the AIS^{28,42}, and was found to be sufficient to obtain neuronal avalanches. We obtained good data collapse and finite-size behavior for the $P_S(S)$ distributions but, in contrast with the static model, we get a finite-size exponent $c_S = 2/3$. The reason for this difference is not clear by now, but we notice that such $c_S = 2/3$ exponent has been found previously in the Pruessner-Jensen SOC model and explained by a field theory elaborated for such systems⁴³.

The great advantage of this new SOC mechanism is its computational efficiency: when simulating N neurons with K synapses each, there are only N dynamic equations for the gains $\gamma_i[t]$, instead of NK equations for the synaptic weights $W_{ij}[t]$. Notice that, for the all-to-all coupling network studied here, this means $O(N^2)$ equations for dynamic synapse but only $O(N)$ equations for dynamic gains. This makes a huge difference for the network sizes that can be simulated.

We stress that, since we used τ finite, the criticality is not perfect ($\gamma^*/\gamma_C \in [1.001; 1.01]$). So, we called it a self-organized superCriticality (SOSC) phenomenon. If $x = 1/(uC\tau) \approx 0.001$, the stationary state is experimentally indistinguishable from true SOC. However, if $x < 100$, large avalanches can be obtained. Interestingly, SOSC would be a concretization of Turing intuition that the best brain operating point is slightly supercritical¹.

We speculate that this slightly supercriticality could explain why humans are so prone to supercritical-like pathological states like epilepsy (prevalence 1.7%) and mania (prevalence 2.6)³. From our mechanism, such pathological states arises from small gain depression u or small gain recovery time τ . These parameters are experimentally related to firing rate adaptation and perhaps our proposal could be experimentally studied in normal and pathological tissues.

We also conjecture that this supercriticality in the whole network could explain the *Subsampling Paradox* in neuronal avalanches: since the initial experimental protocols⁹, critical power laws have been seen when using arrays of $N_e = 32 - 512$ electrodes, that are a very small number compared to the full biological network with $N = O(10^6 - 10^9)$ neurons. This situation $N_e \ll N$ has been called *subsampling*⁴⁴⁻⁴⁶.

The paradox occurs because models that present good power laws for avalanches measured over the total number of neurons N , under subsampling present only exponential tails or log-normal behaviors⁴⁶. No model, to the best of our knowledge, has solved this paradox. Our dynamic gains, since produce supercritical states like $\gamma^* = 1.01\gamma_C$,

could be a solution if the supercriticality in the whole network, described by a power law with a supercritical bump for large avalanches, turns out an apparent pure power law under subsampling. This possibility will be fully explored in another paper.

Directions for future research: Future research could investigate other network topologies and firing functions, heterogeneous networks, the effect of inhibitory neurons^{26,38}, and network learning. The study of self-organized supercriticality (and subsampling) with GL neurons and dynamic neuron gains is particularly promising.

Methods

Numerical Calculations: All numerical calculations are done by using MATLAB software. **Simulation procedures:** Simulation codes are made in Fortran90 and C++11. The avalanche statistics were obtained by simulating the evolution of finite networks of N neurons, with uniform synaptic strengths $W_{ij} = W$ ($W_{ii} = 0$), $\Phi(V)$ monomial linear ($r = 1$) and critical parameter values $W_C = 1$ and $\gamma_C = 1$. Each avalanche was started with all neuron potentials $V_i[0] = V_R = 0$ and forcing the firing of a single random neuron i by setting $X_i[0] = 1$.

In contrast to standard integrate-and fire^{10,11} or automata networks^{4,12,13}, stochastic networks can fire even after intervals with no firing ($\rho[t] = 0$) because membrane voltages $V_i[t]$ are not necessarily zero and $\Phi(V)$ can produce new delayed firings. So, our criteria to define avalanches is slightly different from previous literature: the network was simulated according to equation (1) until all potentials had decayed to such low values that $\sum_i^N V_i[t] < 10^{-20}$, so further spontaneous firing would not be expected to occur for thousands of steps, which defines a *stop time*. Then, the total number of firings S is counted from the first firing up to this stop time.

The correct finite-size scaling for avalanche duration is obtained by defining the duration as $D = D_{bare} + 5$ time steps, where D_{bare} is the measured duration in the simulation. These extra five time steps probably arise from the new definition of avalanche used for these stochastic neurons.

Appendix

The degenerate 2-cycle regimes

If for some Φ there is a saturating potential V_S such that $\Phi(V_S) = 1$, then the fixed point ρ loses stability at some bifurcation point $W = W_B$. The value of W_B can be obtained remembering that, due to the refractory period, the maximal fixed point is $\rho = \rho_B = 1/2$. The bifurcation point is $W_B = 2V_S$ because, at this point, we have $U_1 = V_S$, $\Phi(U_1) = 1$ and $\Phi(U_k) = 0$ for $k > 1$, so that the stationary condition for ρ reduces to $\rho_B = 1 - \rho_B$, i.e. $\rho_B = 1/2$.

When $W > W_B = 2V_S$, besides the solution $\rho = 1/2$, there is an infinitude of solutions where the same potential distribution repeats with period 2 (*2-cycles*), and the activity $\rho[t]$ alternates between $\rho[t] = 1/2 + \varepsilon(W)$ and $\rho[t+1] = 1/2 - \varepsilon(W)$, which are marginally stable. In the $\rho(W)$ curve, these possible periodic states are bounded by the lines:

$$\rho_1(W) = \frac{V_S}{W} \leq \rho \leq \frac{W - V_S}{W} = \rho_2(W), \quad (31)$$

(Fig. 3b). These limits are obtained by using the condition $U_1[t] = W\rho_1(W) = V_S$ and $\rho_2(W) = 1 - \rho_1(W)$.

The degenerate state with $\rho[t+1] = \rho[t] = 1/2$ and the *2-cycles* with $\varepsilon > 0$ are marginally stable because the value of $\varepsilon(W)$ is not unique (for a given W): any value $\varepsilon(W)$ compatible with the limits of equation (31) can occur. These *2-cycles* are not peculiar to the GL model: they also occur in the deterministic LIF model.

Isolated neurons

We analyze the behavior of the GL neuron model under the standard experiment where an isolated neuron in vitro is artificially injected with a current of constant intensity J . That corresponds to setting the external input signal $I[t]$ of that neuron to a constant value $I = J\Delta/C$ where C is the effective capacitance of the neuron.

The firing rate of an isolated neuron can be written as:

$$F(I) = \rho(I)F_{\max}; \quad (32)$$

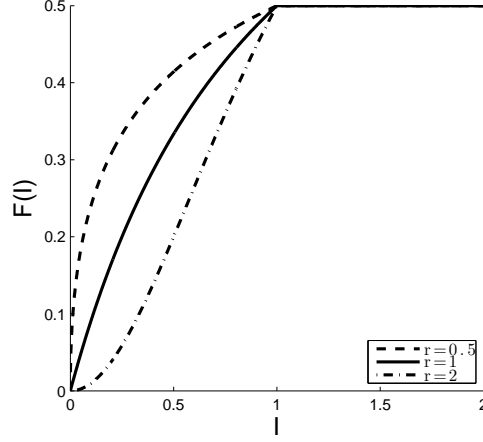


Figure 7. Firing rate of an isolated neuron: $F(I)$ as a function of external input I , for exponents $r = 0.5, 1$ and 2 .

where F_{\max} is the empirical maximum firing rate (measured in spikes per second) of a given neuron and ρ is our previous neuron firing probability per time step. With $W = 0$ and $I > 0$ in equation 16, we get:

$$\rho(I) = \Phi(I)(1 - \rho(I)), \quad (33)$$

The solution for the monomial saturating Φ with $V_T = 0$ is:

$$\rho(I) = \frac{(\gamma I)^r}{1 + (\gamma I)^r}, \quad (34)$$

which is less than $\rho = 1/2$ only if $I < 1/\gamma$. For any $I \geq 1/\gamma$ the firing rate saturates at $\rho = 1/2$ (the neuron fires at every other step, alternating between potentials $U_0 = V_R = 0$ and $U_1 = I$). So, for $I > 0$, there is no phase transition. Interestingly, Eqs. (34), known as generalized Michaelis-Menten function, is frequently used to fit the firing response of biological neurons to DC currents^{47,48}.

Discontinuous phase transitions in networks: the case with $V_T > 0$ and $I > 0$.

The standard IF model has $V_T > 0$. If we allow this feature in our models we find a new ingredient that produces first order phase transitions. Indeed, in this case, if $U_1 = W\rho + I < V_T$ then we have a single peak at $U_0 = 0$ with $\eta_0 = 1$, which means we have a silent state. When $U_1 = W\rho + I > V_T$, we have a peak with height $\eta_1 = 1 - \rho$ and $\rho = \eta_0 = \Phi(U_1)\eta_1$.

For the linear monomial model this leads to the equations:

$$\rho = \gamma(U_1 - V_T)(1 - \rho), \quad (35)$$

$$\gamma W \rho^2 + (1 - \gamma W - \gamma V_T + \gamma I)\rho + \gamma V_T - \gamma I = 0, \quad (36)$$

with the solution:

$$\rho^\pm(\gamma, W, V_T, I) = \frac{(\gamma W + \gamma V_T - \gamma I - 1) \pm \sqrt{(\gamma W + \gamma V_T - \gamma I - 1)^2 - 4\gamma^2 W V_T + 4\gamma^2 W I}}{2\gamma W}, \quad (37)$$

where ρ^+ is the non trivial fixed point and ρ^- is the unstable fixed point (separatrix). These solutions only exist for γW values such that $\gamma(W + V_T - I) - 1 > 2\gamma\sqrt{W(V_T - I)}$. This produces the condition:

$$\gamma W > \gamma W_C = \left(1 + \sqrt{\gamma(V_T - I)}\right)^2, \quad (38)$$

which defines a first order critical boundary. At the critical boundary the density of firing neurons is:

$$\rho_C = \frac{\sqrt{\gamma(V_T - I)}}{1 + \sqrt{\gamma(V_T - I)}}, \quad (39)$$

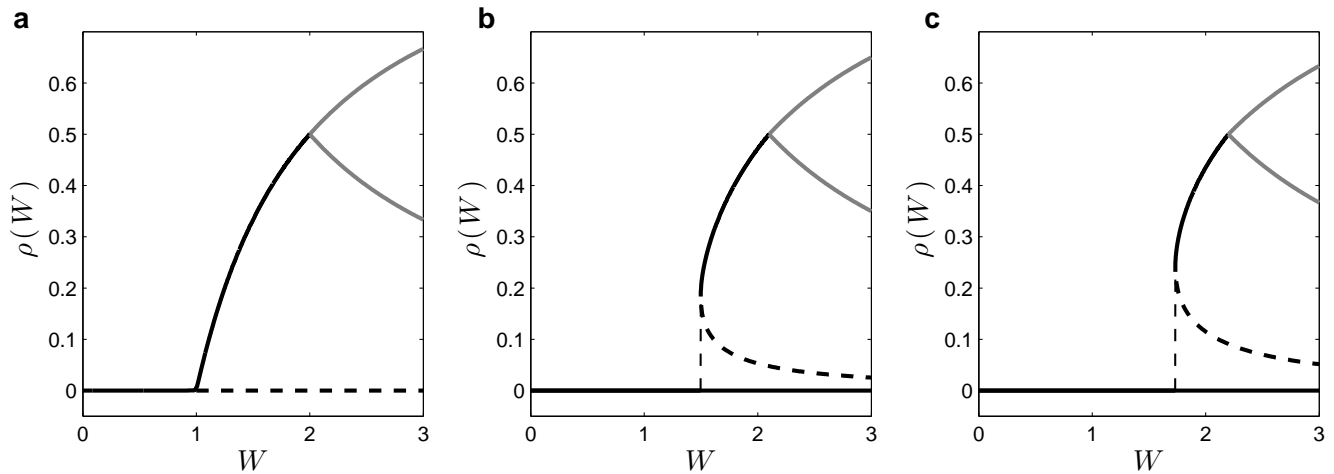


Figure 8. Phase transitions for $V_T > 0$: monomial model with $\mu = 0, r = 1, \gamma = 1$ and thresholds $V_T = 0, 0.05$ and 0.1 . Here the solid black lines represent the stable fixed points, dashed black lines represent unstable fixed points and grey lines correspond to the marginally stable boundaries of cycles-2 regime. The discontinuity ρ_C goes to zero for $V_T \rightarrow 0$.

which is nonzero (discontinuous) for any $V_T > I$. These transitions can be seen in (Fig. 8). The solutions for equations (37) and (39) is valid only for $\rho_C < 1/2$ (2-cycle bifurcation). This imply the maximal value $V_T = 1/\gamma + I$.

References

1. Turing, A. M. Computing machinery and intelligence. *Mind* **59**, 433–460 (1950).
2. Chialvo, D. R. Emergent complex neural dynamics. *Nature physics* **6**, 744–750 (2010).
3. Hesse, J. & Gross, T. Self-organized criticality as a fundamental property of neural systems. *Criticality as a signature of healthy neural systems: multi-scale experimental and computational studies* (2015).
4. Kinouchi, O. & Copelli, M. Optimal dynamical range of excitable networks at criticality. *Nature physics* **2**, 348–351 (2006).
5. Beggs, J. M. The criticality hypothesis: how local cortical networks might optimize information processing. *Philosophical Transactions of the Royal Society of London A: Mathematical, Physical and Engineering Sciences* **366**, 329–343 (2008).
6. Shew, W. L., Yang, H., Petermann, T., Roy, R. & Plenz, D. Neuronal avalanches imply maximum dynamic range in cortical networks at criticality. *The Journal of Neuroscience* **29**, 15595–15600 (2009).
7. Massobrio, P., de Arcangelis, L., Pasquale, V., Jensen, H. J. & Plenz, D. Criticality as a signature of healthy neural systems. *Frontiers in systems neuroscience* **9** (2015).
8. Herz, A. V. & Hopfield, J. J. Earthquake cycles and neural reverberations: collective oscillations in systems with pulse-coupled threshold elements. *Physical review letters* **75**, 1222 (1995).
9. Beggs, J. M. & Plenz, D. Neuronal avalanches in neocortical circuits. *The Journal of neuroscience* **23**, 11167–11177 (2003).
10. Levina, A., Herrmann, J. M. & Geisel, T. Dynamical synapses causing self-organized criticality in neural networks. *Nature physics* **3**, 857–860 (2007).
11. Bonachela, J. A., De Franciscis, S., Torres, J. J. & Muñoz, M. A. Self-organization without conservation: are neuronal avalanches generically critical? *Journal of Statistical Mechanics: Theory and Experiment* **2010**, P02015 (2010).
12. Costa, A., Copelli, M. & Kinouchi, O. Can dynamical synapses produce true self-organized criticality? *Journal of Statistical Mechanics: Theory and Experiment* **2015**, P06004 (2015).

13. Campos, J., Costa, A., Copelli, M. & Kinouchi, O. Differences between quenched and annealed networks with dynamical links. *arXiv:1604.05779* Submitted to Physical Review E (2016).
14. Ermentrout, B., Pascal, M. & Gutkin, B. The effects of spike frequency adaptation and negative feedback on the synchronization of neural oscillators. *Neural Computation* **13**, 1285–1310 (2001).
15. Benda, J. & Herz, A. V. A universal model for spike-frequency adaptation. *Neural computation* **15**, 2523–2564 (2003).
16. Buonocore, A., Caputo, L., Pirozzi, E. & Carfora, M. F. A leaky integrate-and-fire model with adaptation for the generation of a spike train. *Mathematical biosciences and engineering: MBE* **13**, 483–493 (2016).
17. Galves, A. & Löcherbach, E. Infinite systems of interacting chains with memory of variable length—a stochastic model for biological neural nets. *Journal of Statistical Physics* **151**, 896–921 (2013).
18. Lapicque, L. Recherches quantitatives sur l’excitation électrique des nerfs traitée comme une polarisation. *J. Physiol. Pathol. Générale* **9**, 620–635 (1907). Translation: Brunel, N. & van Rossum, M.C. Quantitative investigations of electrical nerve excitation treated as polarization. *Biol. Cybernetics* **97**, 341–349 (2007).
19. Gerstein, G. L. & Mandelbrot, B. Random walk models for the spike activity of a single neuron. *Biophysical journal* **4**, 41 (1964).
20. Burkitt, A. N. A review of the integrate-and-fire neuron model: I. homogeneous synaptic input. *Biological cybernetics* **95**, 1–19 (2006).
21. Burkitt, A. N. A review of the integrate-and-fire neuron model: Ii. inhomogeneous synaptic input and network properties. *Biological cybernetics* **95**, 97–112 (2006).
22. Naud, R. & Gerstner, W. The performance (and limits) of simple neuron models: generalizations of the leaky integrate-and-fire model. In *Computational Systems Neurobiology*, 163–192 (Springer, 2012).
23. Brette, R. *et al.* Simulation of networks of spiking neurons: a review of tools and strategies. *Journal of computational neuroscience* **23**, 349–398 (2007).
24. Brette, R. What is the most realistic single-compartment model of spike initiation? *PLoS Comput Biol* **11**, e1004114 (2015).
25. Benayoun, M., Cowan, J. D., van Drongelen, W. & Wallace, E. Avalanches in a stochastic model of spiking neurons. *PLoS Comput Biol* **6**, e1000846 (2010).
26. Ostojic, S. Two types of asynchronous activity in networks of excitatory and inhibitory spiking neurons. *Nature neuroscience* **17**, 594–600 (2014).
27. Torres, J. J. & Marro, J. Brain performance versus phase transitions. *Scientific reports* **5** (2015).
28. Platkiewicz, J. & Brette, R. A threshold equation for action potential initiation. *PLoS Comput Biol* **6**, e1000850 (2010).
29. McDonnell, M. D., Goldwyn, J. H. & Lindner, B. Editorial: Neuronal stochastic variability: Influences on spiking dynamics and network activity. *Frontiers in computational neuroscience* **10** (2016).
30. Soula, H., Beslon, G. & Mazet, O. Spontaneous dynamics of asymmetric random recurrent spiking neural networks. *Neural Computation* **18**, 60–79 (2006).
31. Cessac, B. A discrete time neural network model with spiking neurons. *Journal of Mathematical Biology* **56**, 311–345 (2008).
32. Cessac, B. A view of neural networks as dynamical systems. *International Journal of Bifurcation and Chaos* **20**, 1585–1629 (2010).
33. Cessac, B. A discrete time neural network model with spiking neurons: Ii: Dynamics with noise. *Journal of mathematical biology* **62**, 863–900 (2011).
34. De Masi, A., Galves, A., Löcherbach, E. & Presutti, E. Hydrodynamic limit for interacting neurons. *Journal of Statistical Physics* **158**, 866–902 (2015).
35. Duarte, A. & Ost, G. A model for neural activity in the absence of external stimuli. *Markov Processes and Related Fields* **22**, 37–52 (2016).
36. Duarte, A., Ost, G. & Rodríguez, A. A. Hydrodynamic limit for spatially structured interacting neurons. *Journal of Statistical Physics* **161**, 1163–1202 (2015).

37. Galves, A. & Löcherbach, E. Modeling networks of spiking neurons as interacting processes with memory of variable length. *J. Soc. Franc. Stat.* **157**, 17–32 (2016).
38. Larremore, D. B., Shew, W. L., Ott, E., Sorrentino, F. & Restrepo, J. G. Inhibition causes ceaseless dynamics in networks of excitable nodes. *Physical review letters* **112**, 138103 (2014).
39. Cooper, S. J. Donald o. hebb’s synapse and learning rule: a history and commentary. *Neuroscience & Biobehavioral Reviews* **28**, 851–874 (2005).
40. Tsodyks, M., Pawelzik, K. & Markram, H. Neural networks with dynamic synapses. *Neural computation* **10**, 821–835 (1998).
41. Larremore, D. B., Shew, W. L. & Restrepo, J. G. Predicting criticality and dynamic range in complex networks: effects of topology. *Physical review letters* **106**, 058101 (2011).
42. Kole, M. H. & Stuart, G. J. Signal processing in the axon initial segment. *Neuron* **73**, 235–247 (2012).
43. Bonachela, J. A. & Muñoz, M. A. Self-organization without conservation: true or just apparent scale-invariance? *Journal of Statistical Mechanics: Theory and Experiment* **2009**, P09009 (2009).
44. Priesemann, V., Munk, M. H. & Wibral, M. Subsampling effects in neuronal avalanche distributions recorded in vivo. *BMC neuroscience* **10**, 40 (2009).
45. Ribeiro, T. L. *et al.* Spike avalanches exhibit universal dynamics across the sleep-wake cycle. *PloS one* **5**, e14129 (2010).
46. Ribeiro, T. L., Ribeiro, S., Belchior, H., Caixeta, F. & Copelli, M. Undersampled critical branching processes on small-world and random networks fail to reproduce the statistics of spike avalanches. *PloS one* **9**, e94992 (2014).
47. Lipetz, L. E. The relation of physiological and psychological aspects of sensory intensity. In *Principles of Receptor Physiology*, 191–225 (Springer, 1971).
48. Naka, K.-I. & Rushton, W. A. S-potentials from luminosity units in the retina of fish (cyprinidae). *The Journal of physiology* **185**, 587 (1966).

Acknowledgements

This paper results from research activity on the FAPESP Center for Neuromathematics (FAPESP grant 2013/07699-0). OK and AAC also received support from Núcleo de Apoio à Pesquisa CNAIPS-USP and FAPESP (grant 2016/00430-3). LB, JS and ACR also received CNPq support (grants 165828/2015-3, 310706/2015-7 and 306251/2014-0). We thank A. Galves for suggestions and revision of the paper, and M. Copelli and S. Ribeiro for discussions.

Author contributions statement

LB and AAC performed the simulations and prepared all the figures. OK and JS made the analytic calculations. OK, JS and LB wrote the paper. MA and ACR contributed with ideas, the writing of the paper and citations to the literature. All authors reviewed the manuscript.

Competing financial interests The authors declare no competing financial interests.